Macromolecules
ARTICLE

Macromolecules **2009**, *42*, 9133–9140 **9133**
DOI: 10.1021/ma901448x

Micelle Morphology and Mechanical Response of Triblock Gels

Michelle E. Seitz,[†] Wesley R. Burghardt,[‡] and Kenneth R. Shull*,[†]

[†]*Department of Materials Science and Engineering, Northwestern University, Evanston, Illinois 60208, and* [‡]*Department of Chemical and Biological Engineering, Northwestern University, Evanston, Illinois 60208*

Received July 3, 2009; Revised Manuscript Received September 17, 2009

ABSTRACT: The effect of polymer concentration on mechanical response and micelle morphology of ABA and AB copolymers in B-selective solvents has been systematically studied. Micelle morphology was determined using a combination of small-angle X-ray scattering, shear, and birefringence while mechanical response at low and high strains was determined using indentation techniques. Self-consistent field theory calculations were used to determine micelle volume fraction profiles and to construct an equilibrium phase map. The transition from spherical to cylindrical micelles increases the triblock gel modulus and energy dissipation. Combining knowledge of gel relaxation time, which determines the rate at which the gel can equilibrate its micelle structure, with the equilibrium phase map allows estimation of the experimental temperatures and time scales over which kinetic trapping will arrest micelle structure evolution. Kinetic trapping enables cylindrical morphologies to be obtained at significantly lower polymer fractions than is possible in equilibrated systems.

Introduction

There is much interest in understanding the link between polymer gel structure and properties such as modulus and toughness. Double network hydrogels have received attention recently for their excellent toughness;[1] however, they have poor fatigue resistance as toughness results from irreversible damage to the covalently bonded network.[2] Ideally, gels would be able to dissipate large amounts of energy during loading to generate high toughness but would also be able to be "healed" so that the dissipative mechanism would be available for subsequent loadings. Thermoplastic elastomer gels consist of ABA triblock copolymers in midblock selective solvents where endblocks aggregate to form spherical glassy micelles that act as high functionality cross-linking points. At very low concentrations these systems form discrete, flowerlike micelles in which the midblock chains form loops.[3−5] As the concentration increases, so does the probability that the midblocks will adopt a bridging configuration which results in the formation of a transient network. Other materials which form transient networks include HEURS[6] (hydrophobically end-capped urethane-coupled poly(ethylene oxides)), reverse pluronics,[5] and supramolecular gels.[7,8] However, it is the easily accessed glass transition temperature of the endblock aggregates in thermoplastic elastomer gels which gives rise their extremely long relaxation times and robust elastic nature at low temperature.

The mechanical response of such thermoplastic elastomer gels with spherical micellar domains has been widely studied.[3,9−14] While thermoplastic elastomer gels demonstrate reasonable toughness,[15] they have relatively low moduli compared to double network hydrogels. Formation of cylindrical, rather than spherical, micelles would be expected to increase the linear modulus as well as the energy dissipated during loading while still retaining some elastic recovery due to bridging midblocks. Because of their thermoreversibility, a heating cycle would heal the gel structure and return it to the original state. While it is well-known that increasing the relative amount of the minority block leads to a transition from spherical to cylindrical micelles in block copolymer melts and solutions,[16] there is limited literature investigating the properties thermoplastic elastomer gels where the endblock aggregates form cylindrical, rather than spherical, micelles.[17]

This paper has two aims. First, to understand the effect of the micellar cross-link morphology on the mechanical response of thermoreversible acrylic triblock alcogels. Second, to map the phase boundary between spherical and cylindrical micelle morphologies in these systems as well as to understand how kinetic trapping of the structure can freeze in nonequilibrium morphologies. We begin with a discussion of block copolymer ordering in solution followed by introduction of the acrylic triblock alcogels studied here. Next, the gel mechanical response as a function of the volume fraction of A in the system will be discussed. Comparisons with AB diblock solutions will be made to further highlight the implications of bridging midblocks and elucidate micellar structure. Shear alignment and birefringence results will be presented to differentiate between spherical and cylindrical micelle morphologies. Next, self-consistent field theory calculations will be used to map the sphere/cylinder phase boundary as a function of gel concentration and temperature. Finally, the effect of kinetic trapping of the endblock aggregates on gel structure will be discussed.

Background

Behavior of Block Copolymers in Solution. For block copolymer melts, microphase separation is driven by the balance of interfacial tension and chain stretching entropy[18] and can be represented on universal phase maps in the $\chi_{AB}N-f_A$ plane, where f_A is the volume fraction of A in the copolymer, χ_{AB} is the Flory−Huggins interaction parameter between A and B segments, N is the degree of polymerization, and the product $\chi_{AB}N$ represents the degree of segregation between the blocks. Changes in temperature are equivalent to moving in a vertical trajectory within the plane. The phase map for symmetric ABA triblock copolymers is similar to that of AB diblocks since they share the same driving force for phase separation.[18]

*Corresponding author. E-mail: k-shull@northwestern.edu.

Published on Web 10/23/2009

While phase separation in the melt is driven by the interaction of A and B monomers, in solution the interactions between solvent (S) and each of the monomers also contribute to the total system free energy and, therefore, can drive phase separation.[19,20] The phase space of block copolymers in solution can be described by a cube with the melt phase map defining two axes and the volume fraction of copolymer in solution, ϕ, as the third axis.[16,21] However, it should be noted that each phase cube corresponds to fixed values of χ_{AS} and χ_{BS}. Hanley et al. propose that ordering of block copolymer solutions can be understood in terms of trajectories across the melt phase map if represented by effective degree of segregation ($\chi_{eff}N$) and microdomain volume ($f_{A,eff}$).[22] The first quantity, $\chi_{eff}N$, takes into account that the presence of even a neutral solvent can change the degree of segregation between the A and B blocks and that in cases of a highly selective solvent the S−A or S−B interactions can dominate A−B interactions. Laurer et al. have shown that even for systems where χ_{AS} drives the phase separation, modest changes in χ_{BS} can change the regions of phase stability.[17] The second quantity, $f_{A,eff}$, recognizes that solvent can be preferentially partitioned, and thus the block fraction should be renormalized to account for the relative microdomain volumes. In neutral solvents, changes in temperature still correspond to vertical trajectories since solvent is equally distributed. If the solvent selectivity changes with temperature (e.g., χ_{AS} or χ_{BS} are functions of temperature), the phase behavior will follow a diagonal trajectory either toward or away from behavior controlled by the copolymer composition.

The phase behavior of copolymers in selective solvents has been extensively studied using AB diblocks[16,21−23] or ABA triblocks in A-selective solvents.[19,24] In these systems, spherical and cylindrical morphologies can be viewed as micelles. Such solutions exhibit viscous behavior unless the concentration is large enough for the micelles to adopt crystalline packing.[21,23,25]

In contrast to systems that form isolated micelles, symmetric ABA triblock copolymers in B-selective solvents are able to form elastic solids, even in the absence of micelle crystallization, due to the ability of B blocks to form bridges between different A domains. The modulus of triblock copolymer gels with discrete spherical micelles can be described using rubber elasticity because the micelles act as cross-linking points and the mechanical response is dominated by the stretching of the bridging midblocks. From rubber elasticity theory, the Young's modulus, E, for an ideal Neo-Hookean material that has been isotropically swollen by solvent is given by[26]

$$E = (3\nu k_B T)\left(f\frac{d^2}{R_0{}^2}\right) \quad (1)$$

where ν is the number density of chains, d is the average distance between cross-links, $R_0{}^2$ is the mean-squared end-to-end distance for an equilibrium solution of molecules with a molecular weight equal to the average molecular weight between cross-links, and f is the fraction of elastically active molecules (equivalent to the fraction of bridging midblocks for a triblock gel). For triblock copolymer gels with discrete spherical micelles, d scales with the average distance between aggregates and reflects stretching of the midblocks due to geometric constraints. For triblock copolymer gels with a midblock concentration in the unentangled regime, eq 1 describes the modulus.[12] In the case of gels containing glassy cylindrical micelles, deformation of the rigid cylinders rather than stretching of the linking midblocks is expected to dominate the mechanical response and eq 1 is not appropriate.

Table 1. Description of Polymers Studied

polymer	A: PMMA [kg/mol]	B: PnBA; T: PtBA [kg/mol]	f_A	PDI
$A_{23}B_{31}A_{23}$	23	31	0.56	∼1.16
$A_{80}T_{51}$	80	51	0.54	∼1.02
A_9	9		1	1.09

Acrylic Triblock Copolymer Gels. Thermoreversibilty of thermoplastic elastomer gels originates from the temperature dependence of the interaction parameter between the endblocks and the solvent, χ_{AS}. Endblock aggregates form at the critical micelle temperature (CMT). As the gel is cooled, the solvent quality for the endblocks worsen and solvent is expelled from the aggregates.[10] Eventually, the still slightly swollen endblocks reach their glass transition temperature (T_g), and the endblocks are effectively locked in place, resulting in an elastic solid.[10] Between the CMT and T_g, the gel is viscoelastic with a relaxation time defined by rate of endblock exchange that varies rapidly with temperature.[11] For poly(methyl methacrylate)−poly(butyl acrylate)−poly(methyl methacrylate) [PMMA−PBA−PMMA] triblocks in alcohols, the CMT is generally less than 100 °C and the endblock T_g is typically above room temperature, although both transition temperatures have block length and concentration dependence. The very rapid, thermally reversible liquid−solid transition makes these acrylic triblocks excellent model systems for studying the link between gel structure and mechanical properties. Homopolymer PMMA shorter than the endblock length can be solubilized into the endblock aggregates and can thus be used to adjust the total fraction of PMMA in a gel.[9]

Experimental Details

Materials. The acrylic triblock copolymer used in this work was provided by Kuraray Co. and was used as received. The diblock studied was synthesized in-house using anionic polymerization (details can be found elsewhere).[10,27] Homopolymer PMMA of 9 kg/mol and a polydispersity index of 1.09 (P1938-MMA) was obtained from Polymer Source, Inc., and was used as received. The polymers studied are summarized in Table 1. The naming convention uses A to refer to PMMA, B to refer to poly(*n*-butyl acrylate) [PnBA], and T to refer to poly(*tert*-butyl acrylate) [PtBA] blocks, with subscript numbers referring to each block's molecular weight in kg/mol. The diblock and triblock studied were selected because they have nearly identical values of f_A which allows comparison of micelle solutions with and without bridging chains between aggregates. The solution behaviors of PnBA and PtBA are very similar. Samples were prepared by dissolving the copolymer in 2-ethylhexanol (2EH), a selective solvent for either PnBA or PtBA, in sealed vials above ∼90 °C and then cooling to room temperature. The boiling point of the solvent is ∼184 °C, and every effort was made to avoid solvent evaporation.

Homopolymer PMMA shorter than the endblock can be solubilized into the micelle core and provides an avenue for increasing the amount of PMMA in a gel sample. Homopolymer A_9 was added to gels containing 27.5 vol % $A_{23}B_{31}A_{23}$ so the weight ratio of homopolyer:endblock was either 1:4 or 1:2. Samples were then sealed, reheated to ∼90 °C to obtain a clear solution, and cooled. They remained clear, indicating no macrophase separation of the homopolymer occurred.

Indentation Experiments. Indentation measures were performed on a homemade apparatus consisting of a cylindrical flat punch indenter of radius 0.4 mm connected to a load cell attached to an inchworm motor. Displacements were measured

via a fiber-optic displacement sensor. Details of the setup can be found in Lin et al.[28] Samples were loaded at a fixed velocity of 10 μm s^{-1} until a predetermined maximum load was reached, and the indenter was immediately retracted at the same rate. The Young's modulus, E, was calculated from the linear portion of the loading curves using[29]

$$\sigma_{avg} = \frac{P}{\pi a^2} = \frac{8E}{3\pi}\frac{\delta}{a} f_c \quad (2)$$

where σ_{avg} is the average stress under the indenter, P is the measured load, a is the radius of the indenter, δ is the measured displacement, h is the thickness of the sample (3.2 mm for these experiments), and f_c is a function that accounts for the geometric confinement of the sample. It is given by[30]

$$f_c = \left(1+1.33\left(\frac{a}{h}\right)+1.33\left(\frac{a}{h}\right)^3\right) \quad (3)$$

Rheology. Rheological measurements were performed on a Paar Physica MCR-300 rheometer with a double-gap Couette (DG26.7) type fixture. Gels were heated above 70 °C and loaded into the fixture. Gels were equilibrated at each measurement temperature, and a strain sweep was performed to identify the linear viscoelastic (LVE) regime. Isothermal frequency sweeps over an angular frequency (ω) range from 0.1 to 100 rad s^{-1} were performed at a constant stress chosen such that the resulting strain was in the LVE regime. Master curves were constructed by shifting the isothermal frequency sweeps along the frequency axis (see Seitz et al. for a detailed explanation and typical curve[11]). From the master curve, a relaxation time, τ, at any given temperature is defined using

$$\tau = \frac{\eta_0 a_T}{G_0} \quad (4)$$

where η_0 and G_0 are the zero shear viscosity and the plateau shear modulus determined respectively from low- and high-frequency regimes at the reference temperature, while a_T is the shift factor for the temperature of interest. The zero shear viscosity is calculated from

$$\eta_0 = \lim_{\omega \to 0} \frac{G''(\omega)}{\omega} \quad (5)$$

Shear Alignment and Birefringence. Gels were cast and loaded into a Linkam CSS-450 shear cell. Samples were heated to 85 °C, held for at least 5 min, and then cooled at 2 °C/min while shearing at a constant rate of 0.5 s^{-1}. Once the sample reached 50 °C, shearing was stopped, and the sample was quenched to room temperature. Because the Linkam lacked active cooling, the sample took ~1 min to reach ~35 °C. However, since the gel relaxation time increases dramatically with decreasing temperature, this quench rate was sufficient to lock in the sheared microstructure.

Birefringence was measured using a HeNe laser with wavelength of 633 nm, with the shear cell located between crossed or parallel polarizers oriented at ±45° relative to the flow direction. Once a sheared sample was quenched and cooled to room temperature, it was heated at 2 °C/min without applied shear, and the light intensity transmitted using both crossed ($I^{\perp}$) and parallel ($I^{\parallel}$) polarizer configurations was monitored to allow normalization of the measured light intensity ($N^{\perp}$). Birefringence was calculated using

$$N^{\perp} = \frac{I^{\perp}}{I^{\perp}+I^{\parallel}} = \sin^2\left(\frac{\pi \Delta n d}{\lambda}\right) \quad (6)$$

where Δn is the birefringence, d is the optical path length (= sample thickness), and λ is the wavelength.

Table 2. Parameters Used in SCFT Calculations

N_A^{tri}	123	χ_{AB}	0.05
N_B^{tri}	190	χ_{AS}	0.7−1.1
N_S	1	χ_{BS}	0.45

Small-Angle X-ray Scattering. Small-angle X-ray scattering (SAXS) experiments were performed at the DND-CAT beamline 5ID-D at Argonne National Lab's Advanced Photon Source. Gel samples were made by casting a heated solution in a washer (1.6 mm thick, 7.6 mm diameter) between two Kapton layers and cooling to room temperature. The scattering vector ($q = 4\pi \sin(\theta/\lambda)$) range covered 0.1−1.0 nm^{-1} using a beam energy of 17 keV. Isotropic patterns were collected on a 2D detector and then integrated over all azimuths to generate one-dimensional $I(q)$ data.

Self-Consistent Field Theory Calculations. Self-consistent field theory (SCFT) calculations were performed using the methodology described by Bras and Shull,[31] and readers are directed to that reference for a full explanation of the procedure used. The calculation treats the solvent as a homopolymer, S, with $N = 1$. Triblock chains were defined to correspond to the experimentally studied $A_{23}B_{31}A_{23}$ triblock normalized by the molar volume of 2-ethylhexanol (156.9 g/cm^3). The interaction parameter between the solvent and the midblock, χ_{BS}, was fixed at 0.45 to represent good solvent conditions. This is consistent with the observed behavior of acrylic triblock/alcohol systems.[31] The interaction parameter between PMMA and PnBA units was assumed to be constant and equal to 0.05. The interaction parameter between the endblocks and the solvent, χ_{AS}, was allowed to vary between 0.7 and 1.1. Gels in 2-ethylhexanol and butanol have very similar behavior, and thus a published temperature dependence of the interaction parameter between PMMA and butanol[32] ($\chi_{AS} = 1.4508-0.0115T$ where T is the temperature in °C) was used to estimate the temperature corresponding to each value of χ_{AS}. Table 2 summarizes the parameters used in the calculations. The free energy of each geometry at fixed χ_{AS} was determined from curves of free energy as a function of system size, and the equilibrium structure was assigned as the geometry with the lowest free energy. It should be noted that the SCFT calculations were performed to determine the equilibrium micelle geometry and volume fraction profiles for a range of conditions and were not used to evaluate the critical micelle temperature or concentration.

Results and Discussion

Structure and Mechanical Response of Triblock Gels. Indentation experiments were performed to determine the mechanical response of triblock gels with polymer volume fractions ranging from 0.09 to 0.33 (corresponding to weight fractions of PMMA from 0.07 to 0.24). Figure 1 plots the Young's modulus, E, and reduced modulus, $E/\nu k_B T$, as a function of PMMA concentration for neat $A_{23}B_{31}A_{23}$ gels as well as gels with added homopolymer. It should be noted that for the range of concentrations studied here the midblocks should be unentangled,[11] and eq 1 is expected to describe the behavior of gels with spherical aggregates. Values of $E/\nu k_B T$ less than 3 reflect a bridging fraction less than 1 (since $d^2/{R_0}^2$ is always greater than 1). At low gel concentration, the micelles are relatively far apart,[11] and the entropy penalty for stretching a midblock chain between micelles is large. As the PMMA concentration increases, $E/\nu k_B T$ also increases. This increase is likely due to an increase in the bridging fraction and possibly to increased stretching of the midblock chains due to packing constraints around the micelle core as the numbers of chains per aggregate increases.[11,31] At PMMA concentrations above ~0.2, the values of $E/\nu k_B T$ become too large to realistically attribute to elastomer-type behavior dominated by deformation of the solvated

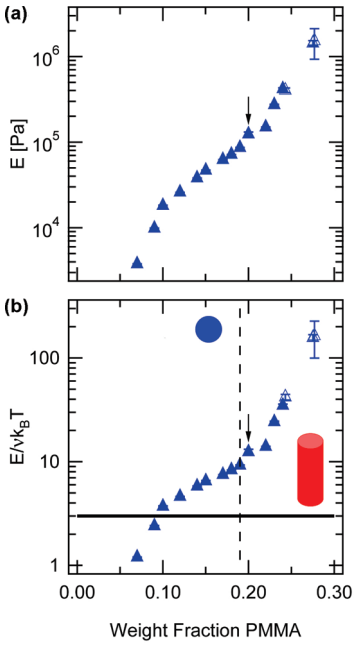

Figure 1. (a) Young's modulus, E, and (b) reduced modulus, $E/\nu k_B T$, as a function of the concentration of PMMA in the gel. Closed symbols correspond to neat $A_{23}B_{31}A_{23}$ gels. Open symbols correspond to nominally 27.5 vol % $A_{23}B_{31}A_{23}$ gels with added A_9 homopolymer. Arrow indicates data point corresponding to neat 27.5 vol % $A_{23}B_{31}A_{23}$ gel. Solid line represents an ideal network ($f(d^2/R_0^2) = 3$). Dashed line represents approximate transition from spherical micelles to cylindrical micelles.

midblocks. The sharp rise in modulus of over an order of magnitude suggests that a different mechanism determining the linear modulus for the higher concentration samples.

To attain higher PMMA weight fractions that were difficult to reach in neat triblock samples due to the large increase in solution viscosity at high concentrations, homopolymer PMMA was added to neat triblock gels. In Figure 1 the base gel concentration to which homopolymer was added and the homopolymer-containing samples are denoted by an arrow and open symbols, respectively. These samples follow the same trend as the neat triblock samples. This indicates that the increase in modulus is being driven by the total PMMA concentration in a sample and not by an increase in network chains because adding homopolymer does not increase the number of network chains (if anything, the increase in micelle core size would be expected to cause a slight decrease in the number of bridging midblocks[33]).

In diblock micellar solutions, a transition from viscous to solid-like behavior is observed with increased concentration due to crystalline packing of the micelles.[21,23,25] Young's moduli for the micellar crystals can be quite high; for crystallized spherical and cylindrical micelles $E \sim 10^3$ and 10^4 Pa, respectively.[23,25] In order to determine whether the increase in modulus observed in concentrated acrylic alcogels is due to crystalline packing of micelles, small-angle X-ray scattering experiments were performed, and scattering patterns are shown in Figure 2.

Scattering contrast in these types of micellar systems arise from electron density differences between the less solvated micelle core and the corona. It is often modeled by treating the system as a random distribution of scatters in a liquid using an approach developed by Kinning and Thomas[34] based on work by Percus and Yevick.[35] In this model, the total scattering intensity is the product of the form factor which accounts for the geometry of the individual micelles

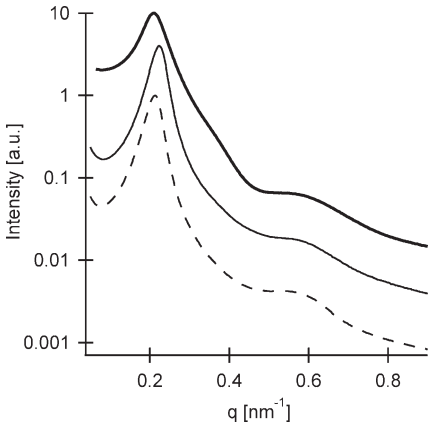

Figure 2. SAXS patterns for triblock gels. Thick and thin solid lines correspond to 13.5 and 27.5 vol % $A_{23}B_{31}A_{23}$ gels. Dashed line corresponds to a nominally 27.5 vol % $A_{23}B_{31}A_{23}$ gel with A_9 added in weight ratio of 1:2 homopolymer:endblock in the sample. Curves have been shifted vertically for clarity.

and the structure factor which accounts for the distribution of micelles in the system. The main peak ($q \sim 0.2$) arises from interaction between micelles and reflects the average distance between scattering centers while the undulations at higher q are related to the form factor of the micelle core. The scattering patterns revealed no higher order reflections for any of the $A_{23}B_{31}A_{23}$ gels in the as-cast state, indicating a random distribution of micelles rather than crystalline packing. The lack of long-range order precludes attributing the sharp increase in modulus to a transition from a random distribution to an ordered array of micelles. If the gel contains randomly distributed glassy, cylindrical micelles, the mechanical response will be dominated by deformation of the cylinders (at least in the linear regime), and rubber elasticity would not adequately describe the linear modulus. It is possible to differentiate between spherical and cylindrical objects by comparing how the intensity decreases with q at relatively large q as $I(q) \sim q^{-\alpha}$ over this range. For spheres and cylinder of uniform density, α equals 4 and 1, respectively.[36] However, in order to determine the value of α with certainty, the power-law behavior should extend over at least a decade in q and the signal-to-noise ratio at high q must be large. Using the data in Figure 2, it is not possible to differentiate between randomly distributed spherical and cylindrical micelles due to the limited q range and the low signal-to-noise at high q.

Figure 3 shows average stress versus normalized displacement from indentation experiments for the initial loading of $A_{23}B_{31}A_{23}$ gels over a range of concentrations. It is clear that the gels behave elastically at the lower concentrations with very little hysteresis over a loading/unloading cycle. However, at higher concentrations the hysteresis becomes much greater. At the highest concentration significant plastic deformation occurs. Laurer et al. observed that triblock gels with cylindrical micelles had much higher moduli and behaved linearly over a much smaller strain range than those with spherical micelles.[17] A transition between spherical and cylindrical micelles as the concentration of PMMA in the gels is increased would, thus, be consistent with the observations in Figures 1 and 3.

Diblock Solution Behavior. Because $A_{80}T_{51}$ and $A_{23}B_{31}A_{23}$ have nearly identical values of f_A, diblock solutions can be studied to better understand the link between micelle morphology and mechanical response. Comparison between diblock and triblock solution behavior can also elucidate the effect of bridging midblocks.

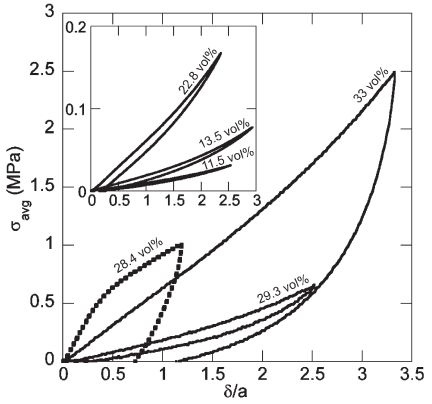

Figure 3. Average stress, σ_{avg}, as a function of the displacement normalized by the indenter radius, δ/a, for $A_{23}B_{31}A_{23}$ gels at 33 and 29.3 vol %. Also included is a 28.4 vol % $A_{80}T_{51}$ sample (dotted line). Inset shows curves for 22.8, 13.5, and 11.5 vol % $A_{23}B_{31}A_{23}$ gels.

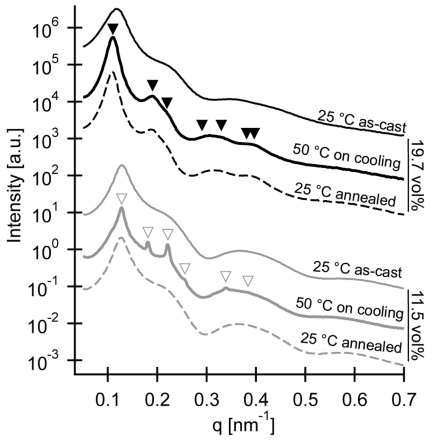

Figure 4. SAXS patterns for 19.7 and 11.5 vol % $A_{80}T_{51}$ solutions. Solid and dashed curves are room temperature patterns before and after annealing at 2 °C/min from 25 to 100−25 °C, respectively. Thick solid lines correspond to scattering at ~55 °C during cooling. Solid and open triangles correspond to allowed reflections for hexagonal ($q = q^*(1, \sqrt{3}, \sqrt{4}, \sqrt{7}, \sqrt{9}, \sqrt{12}, \sqrt{13})$) and BCC ($q = q^*(1, \sqrt{2}, \sqrt{3}, \sqrt{4}, \sqrt{7}, \sqrt{9})$) structures, respectively. Curves have been shifted vertically for clarity.

Solutions of $A_{80}T_{51}$ ranging from 4.7 to 28.4 vol % were prepared. Below 15.6 vol % samples were fluid at room temperature, consistent with isolated micelles. However, above 15.6 vol %, the diblock solutions behaved in a solidlike manner at room temperature (the samples are self-supporting when inverted).

Figure 4 shows SAXS patterns for 11.5 and 19.7 vol % $A_{80}T_{51}$ solutions as cast, after an annealing cycle from 25 to 100−25 at 2 °C/min, and at ~55 °C on the cooling cycle. In the as-cast state, neither sample showed well-defined higher order reflections, consistent with the behavior of the triblock gels. At intermediate temperatures during the annealing cycle, clear higher order reflections appeared. The reflections were consistent with BCC packing of spherical micelles and hexagonal packing of cylindrical micelles for the 11.5 and 19.7 vol % $A_{80}T_{51}$ solutions, respectively. Cooling leads to a loss of ordering in the 11.5 vol % sample. This is likely related to a slight decrease in micelle volume due to reduced solvation of the core. Readers are referred to detailed work by Lodge and co-workers for an expanded discussion of this phenomenon.[24,37]

Indentation experiments were performed on the diblock samples that showed solidlike behavior at room temperature (vol % > 15.6). The response for a 28.4 vol % $A_{80}T_{51}$ sample is included in Figure 3. The diblock samples behave in a plastic manner with clear yielding evident. The loading behavior for the diblock samples is similar to the behavior of the triblock gels at high concentrations; however, triblock gels show significantly greater elastic recovery on unloading.

To further understand the arrangement of cylindrical micelles in higher concentration $A_{80}T_{51}$ samples, solutions were cast and cooled to room temperature before being immersed in a large volume of pure solvent. If the cylindrical micelles were unentangled, immersion in solvent would lead to dispersal of individual micelles into solution. However, if the cylindrical micelles were entangled or defects such as Y-junctions lead to a network of the glassy PMMA phase, the micelles would be hindered from dispersing despite the solvent excess and the sample would remain intact. After several months soaking in pure solvent at room temperature, samples containing at least 19.7 vol % $A_{80}T_{51}$ remained intact, indicating that micelle dispersal was prevented. As differentiation between entanglement and defect junctions is not possible based on the available data, we will use the phrase "entangled cylindrical micelles" to encompass both possibilities.

Triblock Gel Response during Cyclic Loading. To better understand the differences in response between the high and low concentration triblock gels, indentations to a fixed maximum load were repeated in the same location. The results for 33 and 15.6 vol % $A_{23}B_{31}A_{23}$ gels are shown in Figure 5. In Figure 5a, the top of the sample prior to testing corresponds to $\delta/a = 0$, and the shift to larger values of δ/a at the start of subsequent cycles indicates the amount of plastic deformation. Figure 5b plots the same data shifted so that $\delta/a = 0$ corresponds to the top of the sample at the start of each cycle to facilitate comparison of the shape of the curves for each cycle. For the 15.6 vol % gel there is virtually no change in mechanical response between the loading cycles, indicating that the gel response is highly elastic, consistent with a gel structure of isolated spherical micelles. There are several features of the 33 vol % $A_{23}B_{31}A_{23}$ gel's response which differ from that of the lower concentration gel. While the 15.6 vol % gel's response did not change on repeated loading, the 33 vol % sample's response only stabilized after the second loading. The first cycle showed yielding-like behavior, large plastic deformation, and significant energy dissipation. Subsequent loading reveals a softer response as well as decreased dissipation with respect to the first loading. We posit that the 33 vol % $A_{23}B_{31}A_{23}$ sample's response suggest that its structure consists of randomly oriented, entangled cylindrical micelles rather than discrete spherical micelles for the reasons discussed below. The reduced stiffness revealed on subsequent loadings indicates that permanent damage to the gel structure is occurring during the first indentation while the stable response on subsequent loadings indicates no further changes in the structure due to reloading. The elastic recovery upon unloading is attributed to the presence of linking midblocks (while the bridging fraction of midblocks for cylindrical micelles is expected to be reduced compared spherical micelles, it is still significant[18,31]). If endblocks were being pulled from their aggregates, the number of bridging molecules would be reduced and the unloading behavior would evolve with cycling. The similarity in unloading response for each cycle suggests the bridging fraction is unchanged between loadings. A random array of glassy cylinders would account for the oberserved behavior if the cylinders fractured when loaded beyond their elastic limit. Because the indentation experiments are performed below the glass transition of the PMMA aggregates, any

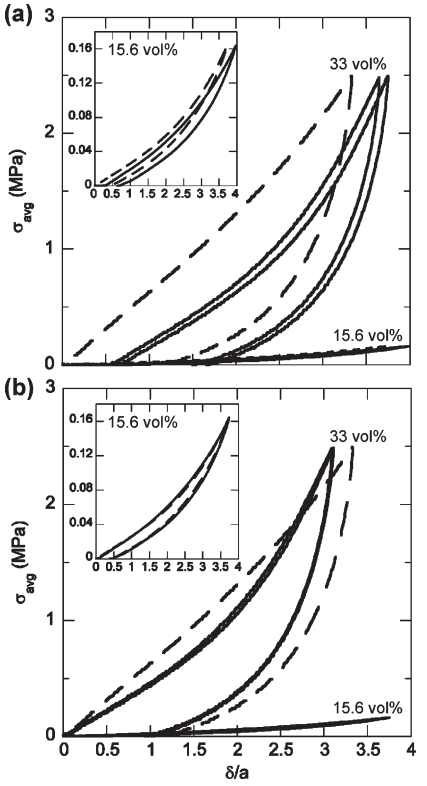

Figure 5. Average stress, σ_{avg}, as a function of the displacement normalized by the indenter radius, δ/a, for 33 and 15.6 vol % $A_{23}B_{31}A_{23}$ gels for repeated loading at the same location with (a) $\delta/a = 0$ corresponding to the top of the sample prior to indentation and (b) data shifted so that $\delta/a = 0$ corresponds to the top of the sample at the start of each cycle. Dotted lines are first indentations, and solid lines are subsequent indentations. Inset shows curves for 15.6 vol % in more detail.

damage to the cylinders will be permanent and irrecoverable at room temperature. Additional dissipation occurs if a subsequent loading exceeds the applied load of the previous loading (data not shown), indicating new damage to the network as the initial load was exceeded consistent with further fracturing of glassy cylinders as the yield stress was exceeded for a larger volume of gel. The assumption of entangled cylinders is also based on similarity in loading behavior between high concentration triblock gels and the cylinder forming diblock solutions.

Shear Alignment and Birefringence. Micelle morphology in concentrated solutions is typically determined via indexing of the higher order reflections from SAXS; however, since our as-cast triblock samples reveal no long-range order, a combination of shear alignment and birefringence was used to differentiate between spherical and cylindrical morphologies.

In the as-cast state, no birefringence was measured for any of the gels, consistent with the isotropic SAXS patterns lacking higher order reflections. It is well-known that block copolymer microdomains in melts or in solution can be aligned by shearing.[20] Because spherical micelles order into cubic crystal structures, they should exhibit no form birefringence under shear. However, cylindrical micelles are anisotropic and should exhibit form birefringence when aligned.

Figure 6 shows a plot of the measured birefringence, Δn, as a function of temperature during quiescent heating at 2 °C/min for 27.5, 22.8, and 13.5 vol % $A_{23}B_{31}A_{23}$ gels quenched from 50 °C after shearing. Also shown are the

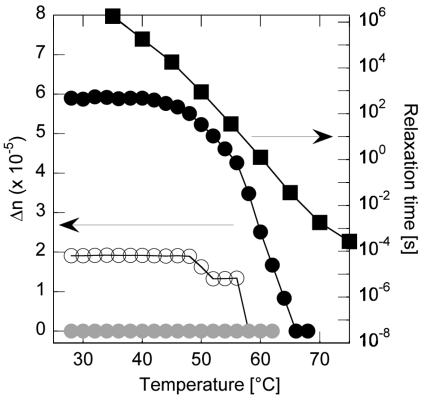

Figure 6. Birefringence, Δn (circles), and relaxation time (squares) as a function of temperature for a shear aligned 27.5 (filled black), 22.8 (open), and 13.5 vol % (filled gray) $A_{23}B_{31}A_{23}$ gels quenched from 50 °C. Birefringence was measured on heating at a rate of 2 °C/min.

relaxation times determined from a rheological master curve for the 27.5 vol % $A_{23}B_{31}A_{23}$ gel. It should be noted that the relaxation times span 10 orders of magnitude over a 40 °C temperature range. As the samples are heated, the birefringence decreases sharply over the temperature range of ~45−65 °C with no measurable birefringence at temperatures above 70 °C. The decrease in birefringence coincides with the decrease in relaxation time. The relaxation time is related to the time scale for stress relaxation in the gel and is a measure of the rate of endblock exchange between micelles.[11] Because no shear is applied during heating, end-block exchange between aggregates causes a loss of global alignment of the micelles and birefringence. If an aligned sample is heated and cooled quiescently, no birefringence is observed after cooling, indicating the reduction in birefringence with temperature is not be solely related to decreased electron density contrast due to micelle swelling but indicates a loss of global micelle alignment.

Diblock samples with spherical micelles (as determined from higher order reflections in SAXS pattern) showed no birefringence either as-cast or under shear, while diblock samples with cylindrical micelles showed birefringence which decayed with temperature in a similar manner to the data shown in Figure 6. Triblock gels with 13.5 vol % $A_{23}B_{31}A_{23}$ showed no birefringence before or after shearing which is consistent with spherical micelles.

It should be noted that the birefringence of microphase-separated block copolymer samples contains contributions due to the shape of the domains (form birefringence) as well as from chain alignment (intrinsic birefringence) and that these contributions can have different signs.[38] Following Lodge and Fredrickson, we estimate the form birefringence for cylindrical micelles using

$$\Delta n_f = (\phi_a {n_a}^2 + \phi_b {n_b}^2)^{1/2} - n_b \left(\frac{(1+\phi_a){n_a}^2 + \phi_b {n_b}^2}{(1+\phi_a){n_b}^2 + \phi_b {n_a}^2} \right)^{1/2} \quad (7)$$

where n is the mean refractive index, ϕ is the volume fraction, and a and b denote the micelle core and corona, respectively. Using n_{PMMA}, n_{PnBA}, and n_{2EH} of 1.49, 1.47, and 1.43, respectively, and $\phi_a = 0.18$ as well as the concentration of solvent in the core and corona from SCFT calculations for a 27.5 vol % $A_{23}B_{31}A_{23}$ gel at room temperature leads to $\Delta n_f = 1e^{-4}$. This value is positive in sign because it is computed relative to the cyclinder axis. Using quarter-wave plates, the sign of the measured birefringence for the shear

aligned 27.5 vol % $A_{23}B_{31}A_{23}$ gel was determined to be negative, indicating that for these systems the intrinsic contribution due to chain alignment is greater than the form contribution to the birefringence. This is consistent with Lodge and Fredrickson's finding that the intrinsic contribution to birefringence in ordered block copolymers is often comparable to or larger than the form birefringence.[38] However, having birefringence dominated by the intrinsic rather than from contribution does not negate the assumption of cylindrical micelles as the instrinsic contribution due to individual chain alignment does not result in observable birefringence in spherical micelles due to their spherical symmetry.

Self-Consistent Field Theory Calculations. Self-consistent field theory calculations were performed in order to map the phase boundary between spherical and cylindrical micellar morphologies for $A_{23}B_{31}A_{23}$ gels in 2-ethylhexanol. As discussed above, the preferential solvent partitioning causes $f_{A,eff}$ to differ from f_A. To correct f_A for preferential solvent swelling, we calculated $f_{A,eff}$ using

$$f_{A,eff} = f_A \phi_p \frac{1}{1-\phi_S} \quad (8)$$

where ϕ_p is the total triblock volume fraction and ϕ_S is the volume fraction of solvent in the core of the micelle. The amount of solvent in the micelle core at a given temperature is nearly identical to the solvent fraction expected for high molecular weight PMMA that is equilibrated with pure solvent. Since the solvent chemical potential, μ_S, is equal to zero when in equilibrium with pure solvent and the core contains only solvent and endblock (e.g., $\phi_S + \phi_A = 1$), the solvent concentration in the core can can be calculated using the Flory−Huggins expression

$$\mu_s = \ln(\phi_S) + (1-\phi_S) + \chi_{AS}(1-\phi_S)^2 = 0 \quad (9)$$

Figure 7a plots the volume fraction profiles as a function of χ_{AS} for a 13.5 vol % $A_{23}B_{31}A_{23}$ gel with spherical micelles. As χ_{AS} increases, ϕ_S changes rapidly and is well described by eq 9 as shown in Figure 7b. Because interactions between solvent and PMMA drive micelle formation in this systems (at least for $\chi_B < 0.5$ which correspond to temperatures of interest in this study), χ_{AS} controls the degree of segregation. We constructed the phase map shown in Figure 8 with χ_{AS} versus $f_{A,eff}$, the effective volume fraction of the PMMA domains. Data points corresponding to systems containing the same volume fraction polymer are connected by dotted lines. Changes in temperature (or χ_{AS}) result in diagonal trajectories across the phase map. As temperature decreases (or χ_{AS} increases), solvent is expelled from the micelle cores driving some systems across the cylinder/sphere phase boundary.

Also included on the phase map are lines corresponding to experimentally measured relaxation times for $A_{23}B_{31}A_{23}$ gels.[11] As the relaxation time increases, the system is unable to exchange endblocks rapidly enough to transform into the equilibrium structure. The kinetic trapping of endblocks has been shown to explain the deviation between micelle size determined from SAXS and that predicted from SCFT.[31] It is clear from Figure 8 that both the low- and high-concentration gels are well within the spherical and cylindrical regions, respectively, for all experimentally accessible temperatures and time scales. In contrast, the intermediate concentration gels cross the cylinder/sphere phase boundary as χ_{AS} increases, and thus the possibility of trapping them

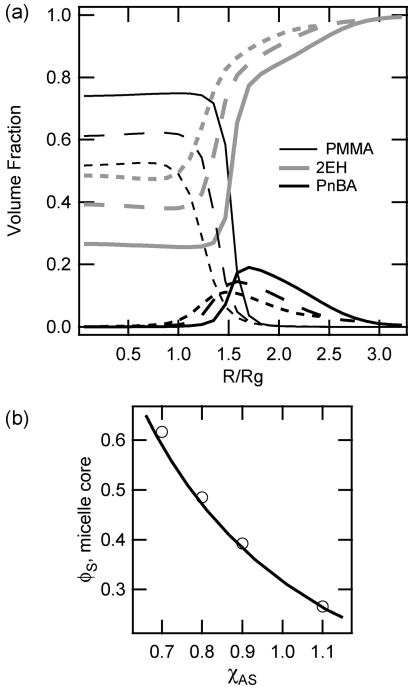

Figure 7. (a) SCFT volume fraction profiles as a function of normalized micelle radius for 13.5 vol % $A_{23}B_{31}A_{23}$ gels. Solid, dashed, and dotted lines correponds to values of χ_{AS} of 1.1, 0.9, and 0.8, respectively. (b) Volume fraction of solvent at the center of the micelle, ϕ_S, as a function of χ_{AS}; symbols correspond to SCFT calculations while the line is eq 9.

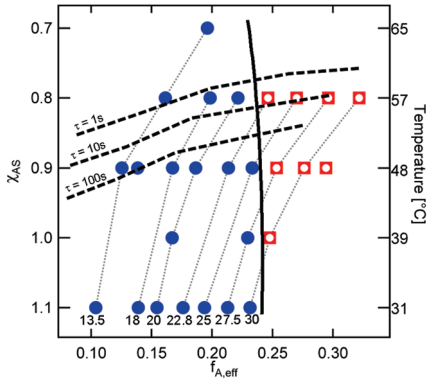

Figure 8. Phase map with χ_{AS} versus $f_{A,eff}$ for $A_{23}B_{31}A_{23}$ gels. Data points corresponding to a fixed triblock concentration are connected by dotted lines and labeled with their corresponding vol % triblock. Filled circles and open squares correspond to equilibrium micelle structures of spheres or cylinders, respectively. The solid line represents the approximate location of the phase boundary between these morphologies. The heavy, dashed lines correspond to gel relaxation times of 1, 10, and 100 s determined from rheological master curves.

in the nonequilibrium cylindrical structure exists. While Figure 8 predicts micelles will be spherical in equilibrium at room temperature for 27.5 and 22.8 vol % $A_{23}B_{31}A_{23}$ gels, both samples had measurable birefringence after shear alignment. Cylindrical micelle structure is preserved at room temperature for these samples due to kinetic trapping as the relaxation times become much larger than the time scale of the experiment. That the birefringence for the 27.5 vol % gel is much larger than that for the 22.8 vol % gel is consistent with quenching from deeper in the cylindrical phase field as well as the increased polymer concentration. The combination of equilibrium phase map with gel relaxation time

highlights the importance of understanding the kinetics of chain exchange for predicting micelle morphology for a given set of experimental cooling rates and time scales.

Conclusions

A systematic study of the effect of triblock concentration on the micelle morphology in $A_{23}B_{31}A_{23}$ gels in 2-ethylhexanol has been presented. The main conclusions are as follows:

1. Triblock gels with cylindrical micelles behave similarly to concentrated diblock solutions with cylindrical micelles and have greater linear modulus and energy dissipation than triblock gels with spherical micelles. However, concentrated triblock gels exhibit significantly more elastic recovery than cylindrical diblocks solutions due to the ability of triblocks to form midblock bridges between micelles.
2. Shear can be used to align cylindrical micelles and leads to birefringence in concentrated triblock gels. The change in birefringence with temperature is correlated with increased endblock exchange between aggregates and a loss of global order.
3. A phase map for the stability of spherical and cylindrical micelles was constructed from self-consistent field theory calculations and accounts for changes in the relative domain volumes due to changes in solvation with temperature changes. Combining knowledge of gel relaxation time which determines the rate at which the gel can equilibrate its micelle structure with the equilibrium phase map determined by SCFT allows estimation of the experimental temperatures and time scales over which kinetic trapping will arrest micelle structure evolution.
4. Kinetic trapping enables cylindrical morphologies to be obtained at substantially lower polymer volume fractions than would be possible in equilibrated systems. For example, the phase map indicates at room temperature cylindrical micelles become the equilibrium phase at > 30 vol % while mechanical testing and birefringence suggest cylindrical micelles are present in room temperature samples with concentrations as low as 23 vol %. The ability to trap cylindrical micelles at lower volume fractions than predicted for equilibrium systems depends on the temperature dependence of χ_{AS} as well as the kinetics of endblock exchange.

Acknowledgment. We are grateful to Kuraray Co. of Japan for providing the triblocks used in these studies and to Steven Weigand for his help collecting the SAXS data. This material is based upon work supported under a National Science Foundation Graduate Research Fellowship and by the Northwestern University Materials Research Center, through the NSF MRSEC program DMR-0520513. Portions of this work were performed at the DuPont-Northwestern-Dow Collaborative Access Team (DND-CAT) Synchrotron Research Center located at Sector 5 of the Advanced Photon Source. DND-CAT is supported by the E. I. DuPont de Nemours & Co., The Dow Chemical Company, the U.S. National Science Foundation through Grant DMR-9304725, and the State of Illinois through the Department of Commerce and the Board of Higher Education Grant IBHE HECA NWU 96. Use of the Advanced Photon Source was supported by the U.S. Department of Energy, Office of Science, Office of Basic Energy Sciences, under Contract W-31-10.

References and Notes

(1) Gong, J. P.; Katsuyama, Y.; Kurokawa, T.; Osada, Y. *Adv. Mater.* **2003**, *15*, 1155–1158.
(2) Webber, R. E.; Creton, C.; Brown, H. R.; Gong, J. P. *Macromolecules* **2007**, *40*, 2919–2927.
(3) Inomata, K.; Nakanishi, D.; Banno, A.; Nakanishi, E.; Abe, Y.; Kurihara, R.; Fujimoto, K.; Nose, T. *Polymer* **2003**, *44*, 5303–5310.
(4) Quintana, J. R.; Janez, M. D.; Katime, I. *Polymer* **1998**, *39*, 2111–2117.
(5) Mortensen, K. *Colloids Surf., A* **2001**, *183*−*185*, 277–292.
(6) Meng, X.-X.; Russel, W. B. *J. Rheol.* **2006**, *50*, 189–205.
(7) Versteegen, R. M.; van Beek, D. J. M.; Sijbesma, R. P.; Vlassopoulos, D.; Fytas, G.; Meijer, E. W. *J. Am. Chem. Soc.* **2005**, *127*, 13862–13868.
(8) Noro, A.; Matsushita, Y.; Lodge, T. P. *Macromolecules* **2008**, *41*, 5839–5844.
(9) Flanigan, C. M.; Crosby, A. J.; Shull, K. R. *Macromolecules* **1999**, *32*, 7251–7262.
(10) Drzal, P. L.; Shull, K. R. *Macromolecules* **2003**, *36*, 2000–2008.
(11) Seitz, M. E.; Burghardt, W. R.; Faber, K. T.; Shull, K. R. *Macromolecules* **2007**, *40*, 1218–1226.
(12) Raspaud, E.; Lairez, D.; Adam, M.; Carton, J. P. *Macromolecules* **1996**, *29*, 1269–1277.
(13) Vega, D. A.; Sebastian, J. M.; Loo, Y. L.; Register, R. A. *J. Polym. Sci., Part B* **2001**, *39*, 2183–2197.
(14) Spontak, R. J.; Patel, N. P. *Curr. Opin. Colloid Interface Sci.* **2000**, *5*, 334–341.
(15) Seitz, M. E.; Martina, D.; Baumberger, T.; Krishnan, V. R.; Hui, C.-Y.; Shull, K. R. *Soft Matter* **2009**, *5*, 447–456.
(16) Huang, C.-I.; Lodge, T. P. *Macromolecules* **1998**, *31*, 3556–3565.
(17) Laurer, J. H.; Khan, S. A.; Spontak, R. J.; Satkowski, M. M.; Grothaus, J. T.; Smith, S. D.; Lin, J. S. *Langmuir* **1999**, *15*, 7947–7955.
(18) Matsen, M. W.; Thompson, R. B. *J. Chem. Phys.* **1999**, *111*, 7139–7146.
(19) Hamley, I. W.; Fairclough, J. P. A.; Ryan, A. J.; Ryu, C. Y.; Lodge, T. P.; Gleeson, A. J.; Pedersen, J. S. *Macromolecules* **1998**, *31*, 1188–1196.
(20) Alexandridis, P.; Spontak, R. J. *Curr. Opin. Colloid Interface Sci.* **1999**, *4*, 130–139.
(21) Lodge, T. P.; Pudil, B.; Hanley, K. J. *Macromolecules* **2002**, *35*, 4707–4717.
(22) Hanley, K. J.; Lodge, T. P.; Huang, C.-I. *Macromolecules* **2000**, *33*, 5918–5931.
(23) Castelletto, V.; Hamley, I. W.; Yuan, X.-F.; Kelarakis, A.; Booth, C. *Soft Matter* **2005**, *1*, 138–145.
(24) Lodge, T. P.; Xu, X.; Ryu, C. Y.; Hamley, I. W.; Fairclough, J. P. A.; Ryan, A. J.; Pedersen, J. S. *Macromolecules* **1996**, *29*, 5955–5964.
(25) Park, M. J.; Char, K.; Lodge, T. P.; Kim, J. K. *J. Phys. Chem. B* **2006**, *110*, 15295–15301.
(26) Ferry, J. D. *Viscoelastic Properties of Polymers*, 3rd ed.; John Wiley & Sons: New York, 1980.
(27) Ahn, D.; Shull, K. R. *Macromolecules* **1996**, *29*, 4381–4390.
(28) Lin, W.-C.; Shull, K. R.; Hui, C.-Y.; Lin, Y.-Y. *J. Chem. Phys.* **2007**, *127*, 094906.
(29) Shull, K. R. *Mater. Sci. Eng. R* **2002**, *36*, 1–45.
(30) Webber, R. E.; Shull, K. R.; Roos, A.; Creton, C. *Phys. Rev. E* **2003**, *68*, 021805.
(31) Bras, R. E.; Shull, K. R. *Macromolecules* **2009**, DOI: 10.1021/ma9013687.
(32) Andrews, E. H.; Levy, G. M.; Willis, J. *J. Mater. Sci.* **1973**, *8*, 1000–1008.
(33) Seitz, M. E.; Rottsolk, R. L.; Shull, K. R. submitted to *J. Polym. Sci., Part B.*
(34) Kinning, D. J.; Thomas, E. L. *Macromolecules* **1984**, *17*, 1712–1718.
(35) Percus, J. K.; Yevick, G. J. *Phys. Rev.* **1958**, *110*, 1–13.
(36) Roe, R.-J. *Methods of X-ray and Neutron-Scattering in Polymer Science*; Oxford University Press: New York, 2000.
(37) Bang, J.; Lodge, T. P. *Phys. Rev. Lett.* **2004**, *93*, 245701.
(38) Lodge, T. P.; Fredrickson, G. H. *Macromolecules* **1992**, *25*, 5643–5650.